JOURNAL OF MATERIALS SCIENCE 14 (1979) 1717–1732

Relationship between surface tension and energy, interfacial energy and lattice friction

K. JAGANNADHAM, M. J. MARCINKOWSKI
Department of Mechanical Engineering, and Engineering Materials Group, University of Maryland, College Park, Maryland 20742, USA

Any surface, in order to decrease its surface energy, contracts. It is shown for the first time that this contraction is formally equivalent to the introduction of a continuous distribution of surface dislocations. Equilibrium is attained when the increase in strain energy associated with these surface dislocations just balances the corresponding decrease due to the reduction in free surface area. Numerical calculations have been carried out for finite solid and liquid bodies as well as for liquid droplets in contact with solids. These findings suggest that it is possible to reformulate the behaviour of liquids in terms of dislocation theory in a much more general way than has hitherto been done.

1. Introduction

One of the most important properties of a body involves the nature of its surface. It also seems clear that a free surface is just a special case of a more general surface such as a two-phase interface or a grain boundary. It has also been shown that internal and external surfaces have associated with them not only surface energy but surface dislocations as well [1–3]. Thus far, however, these studies have not been extended to an internally stress-free body, either a solid or a liquid. It is the purpose of what follows to provide a unified approach to such problems and to show their power, particularly with respect to the liquid state.

2. Surface tension as applied to solid bodies

The solution to any physical problem involves, for the most part, getting the geometry right. We will, therefore, pay particular attention to this important aspect of the study. To begin with, consider the reference state body shown in Fig. 1a which will be denoted by upper case Latin letters, i.e. the (K) state. The (K) state crystal may be separated or torn along the vertical dotted line to generate the (K^T) state crystal shown in Fig. 1b which consists of two newly created free surfaces shown dotted. If a reference or Burgers circuit denoted by the path 1-2-3-4-5-6-1 is taken with respect to the (K) state crystal of Fig. 1a, it becomes the paths 1′-2-3-4′-1′ and 1-4-5-6-1 in the (K^T) state crystal of Fig. 1b. The dotted arrows along the lengths 4-1 and 1′-4′ in Fig. 1b, which correspond to closure failures in the circuit, measure the amount of newly created free surface occasioned by the tearing process. It is important to note that the measure of length or metric tensor a_{KL} is unaltered by the tearing process, where a_{KL} is related to distance ds as follows

$$(ds)^2 = a_{KL}\,dx^K dx^L \qquad (1)$$

and where dx^K are simply co-ordinates, i.e. the number of spacings between two given points. For example, dx^2 corresponding to the distance 5-6 in Fig. 1a is simply 4.

The dotted surfaces in Fig. 1b are assumed to possess no surface energy and therefore remain unaltered by the tearing process. If, however, this restriction is lifted, the (K^{TT}) configuration shown in Fig. 1c obtains. In particular, in order to reduce the surface energy associated with the newly created free surfaces, they try to reduce their length. This, in turn, is opposed by the matter within the body where such considerations do not apply. The torn bodies thus undergo elastic distortion near their free surfaces which can be

0022–2461/79/071717–16 $3.60/0

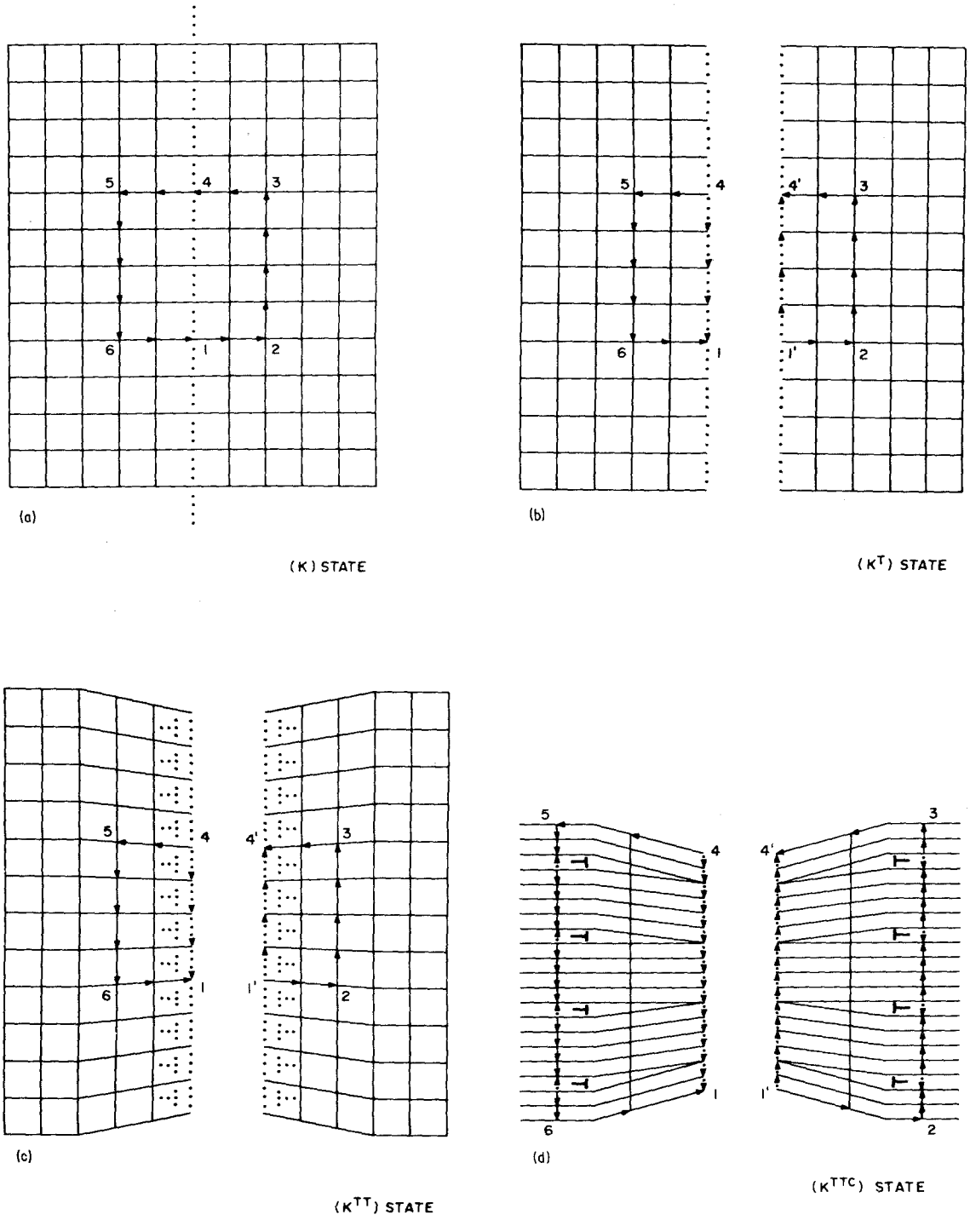

Figure 1 (a) Perfect reference state body. (b) (K) state configuration of (a) after perfect tearing with surface tension absent. (c) (K^T) state configuration of (b) but with surface tension present. (d) (K^{TT}) state configuration of (c) redrawn in terms of a common lattice.

represented in terms of a uniform array of virtual surface dislocations shown dotted in Fig. 1c. The dislocations are termed virtual since they have no extra half planes associated with them [4]. The distortions associated with the surface tension are, in fact, elastic and can be represented by a strain tensor e_{KL} defined as follows [5]:

$$e_{KL} = \tfrac{1}{2}(b_{KL} - a_{KL}) \tag{2}$$

where $b_{K\,L}^{TT\,TT}$ is the metric tensor associated with the (K^{TT}) state. The metric tensor can always be found from the following relationship:

$$b_{K\,L}^{TT\,TT} = e_K^{TT} \cdot e_L^{TT} \tag{3}$$

where e_K^{TT} are the base vectors associated with the (K^{TT}) state which, as is evident from Fig. 1c, are not always unit vectors.

The characteristic feature of an elastic distortion is that it may be represented in terms of a varying metric tensor $b_{K\,L}^{TT\,TT}$ which depends upon position. On the other hand, any elastic distortion may be represented in terms of dislocations [6]. This is most easily seen by reference to Fig. 1d which shows that portion of Fig. 1c within the reference circuit, but represented in terms of a different co-ordinate system. This will be denoted as state (K^{TTC}). It is apparent that the $(K^{TT}) \rightarrow (K^{TTC})$ state transformation is simply a co-ordinate transformation given by $C_{K\,TTC}^{K\,TT}$ which connects the co-ordinates and base vectors as follows:

$$dx^{K\,TTC} = C_{K\,TT}^{K\,TTC}\, dx^{K\,TT} \tag{4a}$$

and

$$e_K^{TTC} = C_{K\,TTC}^{K\,TT}\, e_{K\,TT} \tag{4b}$$

where

$$C_{K\,TTC}^{K\,TT} C_{K\,TT}^{L\,TTC} = \delta_{K\,TTC}^{L\,TTC}, \tag{5}$$

and where $\delta_{K\,TTC}^{L\,TTC}$ is simply the Kronecker delta. The transformation tensor $C_{K\,TTC}^{K\,TT}$ is chosen such that the (K^{TTC}) state of Fig. 1d possesses a common metric tensor, except, of course in the vicinity of the dislocation cores. The imposition of a common metric is also equivalent to the imposition of a common reference lattice. This reference lattice, shown in Fig. 1d, can be subdivided indefinitely, in which case the dislocation array becomes continuous. In the case of Fig. 1d, however, there are only four dislocations between points 5-6 and 2-3 as indicated by the dotted arrows. Since the $(K^{TT}) \rightarrow (K^{TTC})$ transformation is merely a co-ordinate transformation, the strain tensor associated with it vanishes. In terms of Fig. 1d, therefore, surface tension is seen to arise from an array of surface dislocations which form so as to reduce the length of free surface and thus lower the surface energy. It is important to note that in this model, surface tension and surface energy are two separate but interrelated concepts. Fig. 2 shows the atomistic counterpart of the continuous model depicted in Fig. 1d. It is important to note here that the extra half plane associated with each of the two free surfaces is in part uniformly distributed over both these surfaces in agreement with the dislocation representation of Fig. 1d.

3. Interfacial tension as applied to solid bodies

Let us now consider the elastically strained (κ) state shown in Fig. 3a which will be designated by lower case Greek letters. It may be visualized as being generated from the (K) state of Fig. 1a by having the rightmost half of the body undergo a phase change. The phase change is such that the vertical dimensions of the body decrease in length. It is also clear from Fig. 3a that the two phases are perfectly coherent across the interphase boundary, i.e. the displacements are continuous across the boundary. It is also possible to represent the distortion across the boundary in terms of an array of virtual dislocations shown dotted in much the same way as was done in Fig. 1c. Since these are not real dislocations, the reference circuit

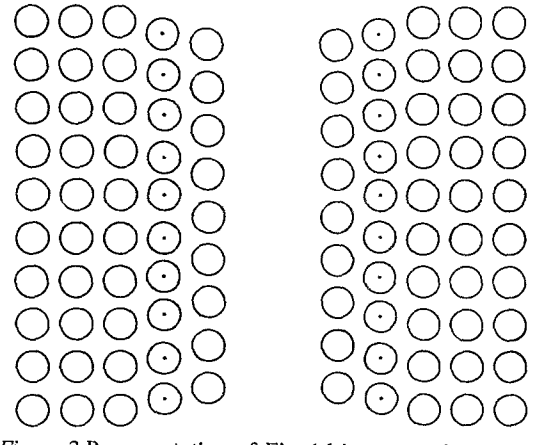

Figure 2 Representation of Fig. 1d in terms of a discrete atomistic picture.

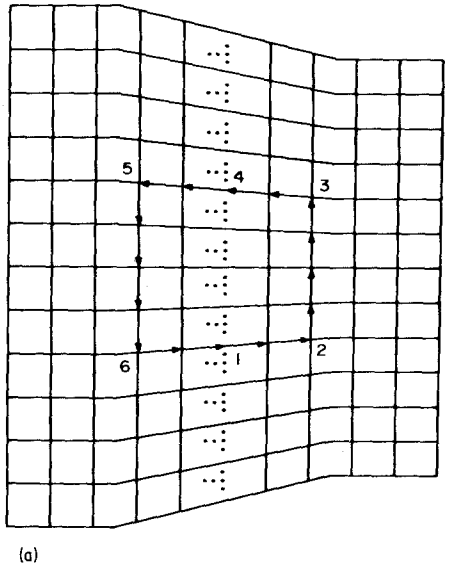

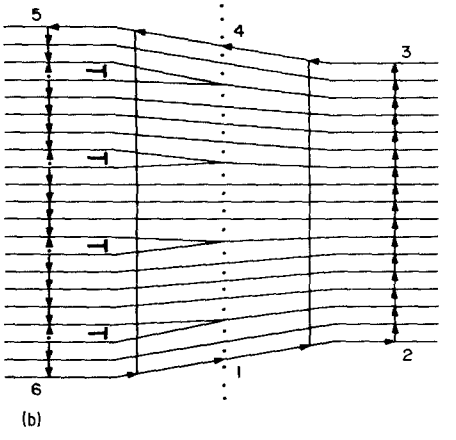

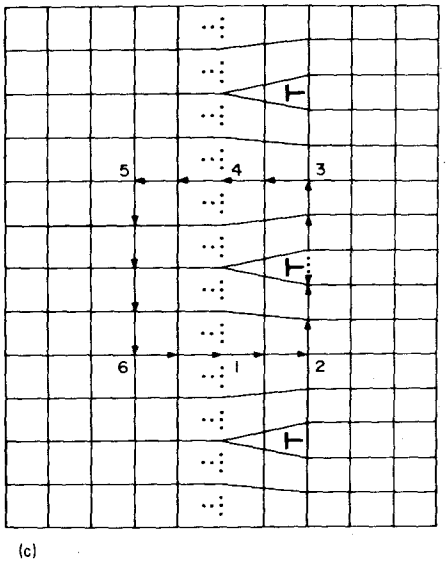

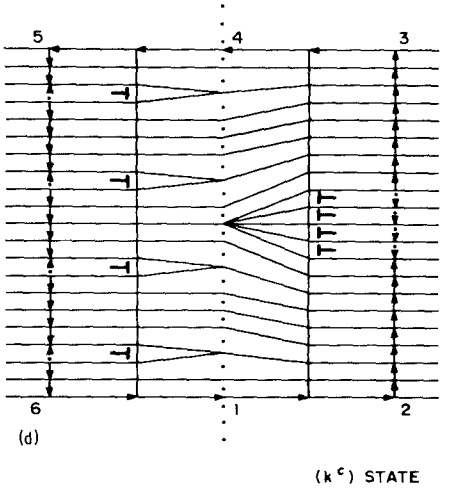

Figure 3 (a) Fully coherent two-phase interface boundary. (b) (κ) state configuration of (a) drawn in terms of a common lattice. (c) (κ) state configuration of (a) after addition of crystal lattice dislocations to remove long range strains. (d) (k) state configuration of (c) drawn in terms of a common lattice. (e) (k) state configuration of (c) after complete annihilation of misfit and interface dislocations. (f) (k^{Γ}) state configuration of (e) drawn in terms of a common lattice. (g) Semi-coherent configuration intermediate between those shown in (c) and (e). (h) (κ) state configuration of (a) after perfect tearing with surface tension present.

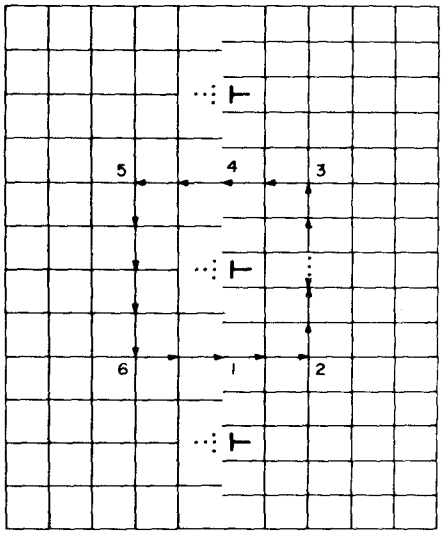

(e)

(k^I)

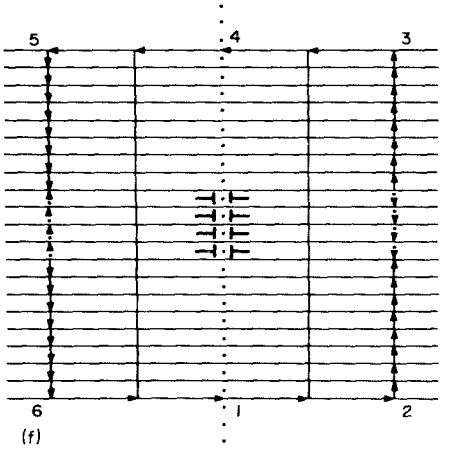

(f)

(k^{IC}) STATE

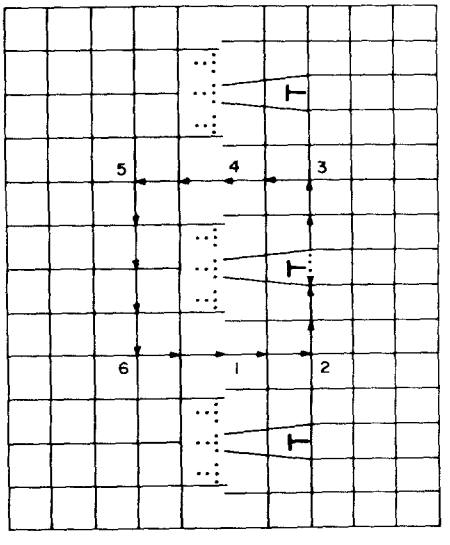

(g)

(k^S)

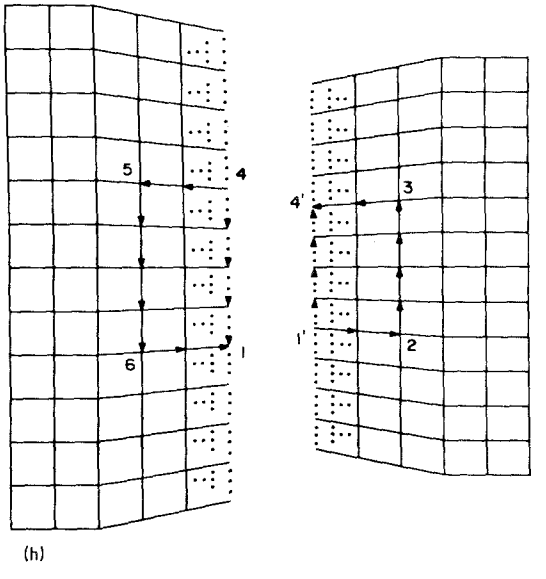

(h)

Figure 3 continued.

1-2-3-4-5-6-1 in Fig. 3a contains no closure failure. However, similar to Fig. 1d, we are able to construct a common lattice as shown in Fig. 3b where it is now possible to represent the coherent two-phase interface in terms of an array of surface dislocations, or perhaps more appropriately, an array of interface dislocations.

The coherent interface of Fig. 3a contains long-range strains which can be removed by the addition of misfit dislocations, which are in fact crystal lattice dislocations (CLD), to the right-most phase as shown by the solid dislocation symbols in Fig. 3c. Such states that contain misfit dislocations will be denoted by lower case Latin letters, i.e. (k). As anticipated, the Burgers circuit in Fig. 3c picks up the single misfit shown by the dotted arrow along line 2-3, but fails to detect the virtual dislocations. If, however, the (k) state is represented in terms of a common lattice by some suitable co-ordinate transformation, the (k^c) state shown in Fig. 3d obtains. It follows from this figure that the misfit dislocations of strength four is just balanced by four interface dislocations, thus accounting for the absence of long-range distortions. Important to note is that the interphase boundaries in Fig. 3c and d, in spite of the fact that they contain misfit dislocations, are still fully coherent. The boundary, however, can be made fully noncoherent by allowing the virtual dislocations in Fig. 3c to combine with the misfit dislocations so as to generate the (k^I) state configuration shown in Fig. 3e. The Burgers circuit portion of this same figure is again reproduced in Fig. 3f but in terms of a common lattice. Note that since the interface dislocations of opposite sign combine completely with one another, as contrasted with Fig. 3c and d, all traces of elastic distortion are removed. The configurations of Fig. 3c and d, on the one hand, and Fig. 3e and f on the other, represent limiting cases of arbitrarily large and vanishingly small interface energies, respectively. In the former case, the interface dislocations cannot move since they create faults, i.e. the atoms are not in line with one another across the interface. In the latter case, they move with no restriction since this energy is vanishingly small. In the case of intermediate interfacial energy, the (k^s) state configuration shown in Fig. 3g obtains. Here, only a portion of the interface dislocations move to the misfit dislocations and annihilate with it [2]. The reconstruction of Fig. 3g in terms of a common lattice is rather straightforward and will therefore be omitted.

It is now clear at this point that the non-alignment of atoms across the boundary in Fig. 3e and g gives rise to an interphase energy which is analogous to the surface energy of Fig. 1c. Since this energy also restricts the movement of interface dislocations, it may also be viewed as giving rise to a lattice friction force acting on these dislocations. Finally, for completeness, Fig. 3h shows the perfectly torn state of Fig. 3a. The surface tension has caused the length of both surfaces to decrease with the subsequent generation of surface dislocations in much the same manner as that described for the perfect reference body of Fig. 1c. Analogous tearing could also be performed on the states shown in Fig. 3b to g with and without surface tension present to yield similar results which, for convenience will be omitted here.

4. Analysis of the surface energy associated with a finite solid of arbitrary shape

A discrete dislocation analysis of the surface energy associated with a finite body is based on the earlier models developed for an externally applied stress or for an internal source of stress [3]. It has been verified therein that the distortion arising from any source of stress in a finite solid can be represented in terms of two sets of surface dislocations with mutually orthogonal Burgers vectors situated on the surface of the solid [1, 7].

The elastic stress field within a finite body due to the effects of surface energy can be obtained by first considering an infinite stressed body. A region within the infinite body, ABCD, of the same dimensions as the finite body is chosen as shown in Fig. 4a. The attractive force offered by the surrounding medium on the surface of the finite region ABCD is illustrated by the arrows corresponding to the component σ_{yy}. The ideas developed using this particular stress component are also applicable to the other components of stress. Fig. 4a shows schematically the two dislocation arrays required to maintain continuity of displacements in the finite region and around it. While such arrays are present everywhere along the boundary of the region ABCD, only one set is shown in order to simplify the figure. The two dislocations to the right of the boundary belong entirely to region ABCD while the two to the left of the boundary belong to the infinite

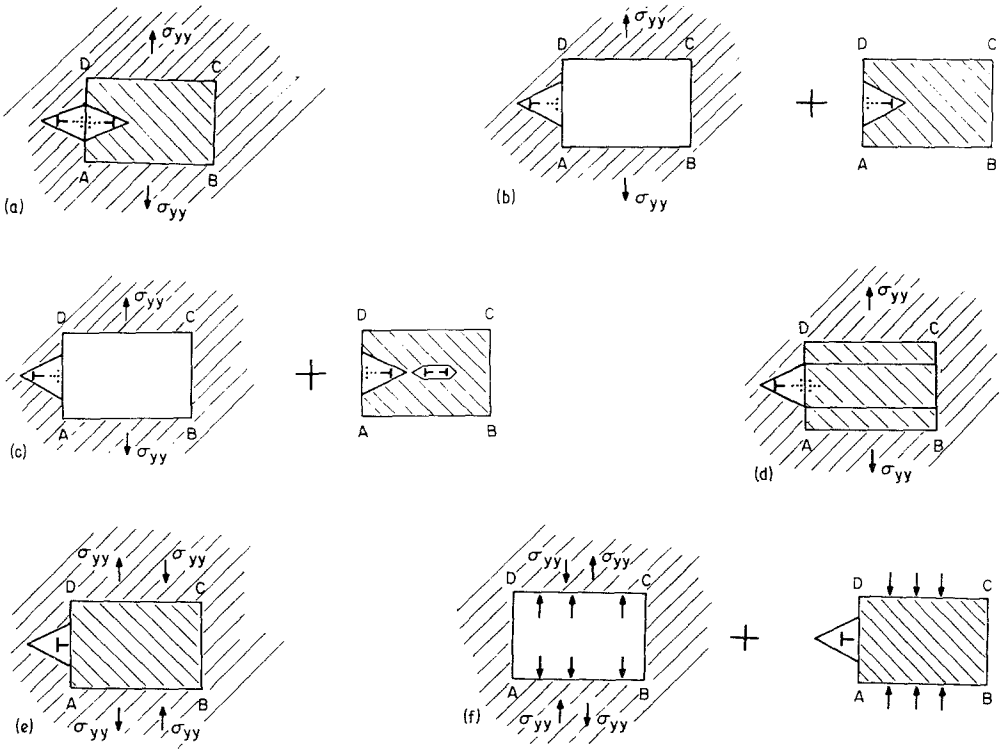

Figure 4 (a) Schematic illustration of the two surface dislocation arrays in region ABCD and surroundings which form in order to maintain continuity of displacements and to satisfy the surface boundary conditions. The dotted symbols correspond to that portion of the dipole which decreases the free surface area. The full line representation corresponds to the edge dislocations which are responsible for the stress field. (b) The finite region is cut from the infinite region and separated from it. (c) Same as (b) except that a prismatic loop is nucleated in the finite region ABCD and allowed to expand and annihilate with a dislocation in the dipole and form an extra plane of material. (d) The finite region is inserted back into the infinite medium. (e) Same as (d) but after a reverse stress is applied to eliminate the dislocations of opposite sign. (f) The finite region ABCD is removed and opposite stresses maintained in order to satisfy the boundary conditions on the surface of the hole ABCD. The surface arrays are distributed on the surface of the finite region to yield the required stress field.

body. Of the two dislocations, the one with the dotted representation corresponds to the reduced free surface [7] while the one with the full line representation gives the stress field. The surfaces are now stress free so that the region ABCD can be cut from the infinite body, as shown in Fig. 4b. A prismatic loop is next introduced into the finite region ABCD so that when the prismatic loop expands, the dislocations with opposite signs annihilate, in turn leaving a dislocation on the surface, as shown in Fig. 4d. Now the finite region ABCD can be inserted back into the infinite body as shown in Fig. 4d. As a next step, the infinite body is subjected to reverse stresses so that the finite region will now be associated with the dislocation array, as shown in Fig. 4e. Finally, the finite region ABCD containing the dislocation array is taken out of the infinite body with opposite stresses maintained on the surfaces of the hole in the infinite body, as shown in Fig. 4f. The region ABCD containing the surface dislocation array, now represents the state of stress in a finite body with constant compressive stresses. The stress field due to the dislocation array on the surface of the finite body balances the compressive stress arising from the absence of the surrounding medium which, in turn, is also the same as the effect of surface energy. It is useful at this stage to employ a different notation to indicate the origin of the stress, namely σ_{ij} which arises due to the presence of surface dislocations and σ^{s}_{ij} as that arising from the absence of the surrounding medium. These two are equal on the surface as shown in Fig. 4f. The fundamental relation between the dislocations and the surface energy is easily obtained by considering the total

energy of the medium, which consists of the strain energy and the surface energy. The strain energy term can be written in its most general form as

$$E_e = \tfrac{1}{2}\int_v \sigma_{ij}e_{ij}\mathrm{d}v = \tfrac{1}{2}\int_s \sigma_{ij}u_i n_j \mathrm{d}s$$

where v is the volume of the solid and s is the surface area surrounding the solid. It is useful to know that σ_{ij} in the volume integral corresponds to the stress everywhere within the finite region, while this same quantity in the surface integral corresponds to the stress on the surface. It is the surface integral representation which is helpful in relating the effect of surface energy to surface stress. The surface energy contribution can be put in the form

$$E_\gamma = -\int_s \gamma \mathrm{d}s.$$

The equilibrium configuration is obtained by noting

$$\frac{\mathrm{d}Ee}{\mathrm{d}s} + \frac{\mathrm{d}E\gamma}{\mathrm{d}s} = 0 \quad \text{so that} \quad \sigma_{ij}u_i n_j = \gamma. \tag{6}$$

In Equation 6, $\sigma_{ij}n_j$ is the force per unit area acting on a plane whose normal is n_j, and $F_i u_i$, where $F_i = \sigma_{ij}n_j$, has the dimensions of force per unit length, the same as that for surface tension. Specifically, for $i = 1$, Equation 6 can be written as

$$\sigma_{11}u_1 n_1 + \sigma_{12}u_1 n_2 = \gamma. \tag{7}$$

The above equation is valid for a finite solid. If the finite region corresponds to that of a liquid, the shear stress components vanish, i.e. $\sigma_{12} = 0$ so that $\sigma_{11}u_1 n_1 = \gamma$ indicating that only hydrostatic stresses maintain the surface tension within a liquid of finite dimension.

The fundamental relation given by Equation 6 between the stresses in a solid and the surface tension can also be reformulated in terms of dislocations arising from surface energy effects as illustrated in Fig. 4f. The stress field due to the dislocation array on the surface gives rise to the strain energy within the finite medium and the decrease in surface associated with the dislocations accounts for the decrease in surface energy. Previous dislocation models of surface tension [8] involved the presence of crystal dislocations situated at some distance from the surface by two or three atoms. This restriction becomes somewhat artificial in view of the definition of a surface dislocation which can, in fact, remain on the surface and not necessarily have associated with it an extra half plane of atoms, i.e. be in the form of a crystal lattice dislocation. The discrete dislocation analysis is carried out by minimizing the total energy required to introduce surface dislocations onto the surface. In particular

$$E_\mathrm{T} = E_e + E_\gamma \tag{8}$$

where

$$E_e = E_\mathrm{S} + E_\mathrm{I}, \quad \text{so that} \quad E_\mathrm{T} = E_\mathrm{S} + E_\mathrm{I} + E_\gamma, \tag{9}$$

where E_S is the self energy and E_I the interaction energy of the dislocation array while E_γ corresponds to the increase in surface energy due to presence of the dislocations. These results may be illustrated for the array with Burgers vector parallel to the surface for which

$$E_\mathrm{S} + E_\mathrm{I} = \sum_{i=1}^{N}\int_{-R}^{x_i} \tau_{xy}\boldsymbol{b}_i \mathrm{d}x_i = \sum_{i=1}^{N} \tau_{xy}\boldsymbol{b}_i x_i \tag{10}$$

where N is the total number of dislocations, R is the size of the crystal, and τ_{xy} the shear stress acting on each dislocation. The dislocation with Burgers vector $\boldsymbol{b}_i$ is considered as being brought from infinity to the position x_i. For simplicity in the above equation, τ_{xy} is assumed to be constant. The surface energy lost due to the formation of the dislocations can be written as

$$E_\gamma = -\sum_{i=1}^{N} \gamma \boldsymbol{b}_i. \tag{11}$$

If τ^s_{xy} is the shear stress arising from surface energy effects, namely that represented by arrows pointing towards the finite region ABCD in Fig. 4f, the above equation takes the alternate form

$$E_\gamma = -\sum_{i=1}^{N} \tau^\mathrm{s}_{xy}\boldsymbol{b}_i x_i. \tag{12}$$

The total energy of the configuration E_T given by Equation 8 can be minimized with respect to the Burgers vectors and postion co-ordinates of each dislocation so that $\tau_{xy} = \tau^\mathrm{s}_{xy}$, i.e. the shear stress due to the array is balanced by the surface shear stress due to surface energy. Similar reasoning can be extended to the other components of the stress field.

The results shown in Fig. 5a indicate that the

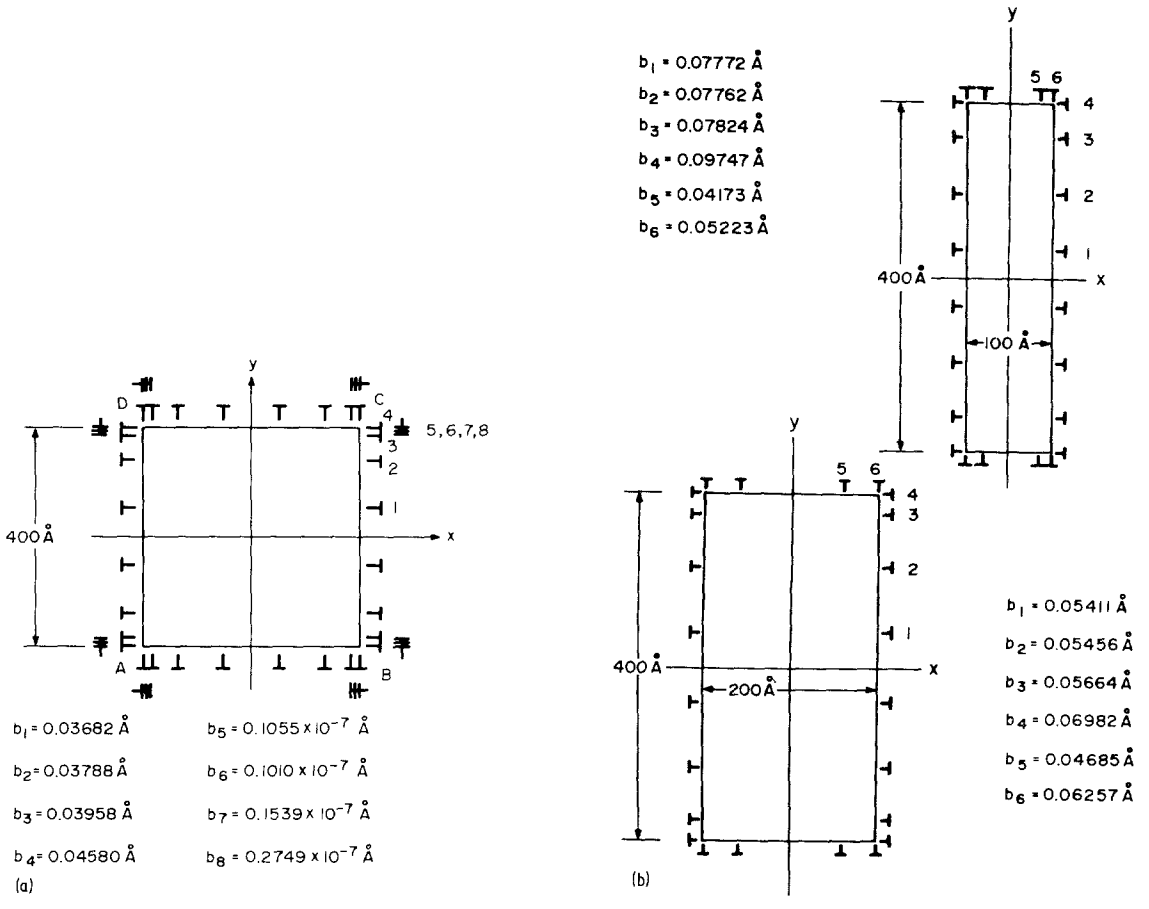

Figure 5 (a) Surface dislocation arrays obtained using the discrete dislocation method of analysis of surface energy. The numbers shown beside each dislocation are used as a subscript to b to indicate the Burgers vector. The value of the Burgers vector of each dislocation is shown. The arrays on all the four faces occupy identical positions due to the symmetry of the square body. The dislocations with numbers 5 and 6 are very close so that they are represented as one. (b) Same as (a) except that the finite body is rectangular and the secondary array is absent. Two bodies with different width are shown.

major effect of surface energy is to generate a dislocation array with Burgers vectors parallel to the surface, also called the primary array. The dislocations in the array with Burgers vectors perpendicular to the surface have very small Burgers vectors and for this reason are called the secondary array. The results of the discrete dislocation analysis for a body with rectangular shape are shown in Fig. 5b where only the primary array is determined since the secondary array has negligible Burgers vector. The primary array is again found to remain uniform except at the corners. It can also be concluded that the Burgers vector of the array increases with decreasing thickness of the finite body as seen from Fig. 5b. The σ_{xy} component of stress for the arrays shown in Fig. 5a and b is plotted as shown in Fig. 6a and b, respectively. These shear stresses are seen to become smaller in the interior of the finite body. The stress level in a finite body with smaller thickness is higher due to the larger Burgers vector of the primary array. Fig. 6c shows the σ_{xx} component of stress due to the array given in Fig. 5a. The stress level again falls off rapidly with distance from the surface. The above results enable us to conclude that the stress components on the surface of a finite solid reach a value equal to the surface stress developed due to the presence of surface energy. However, the stress components decrease rapidly from the surface of the finite body into the interior.

4.1. Numerical analysis of the surface energy associated with a liquid of finite dimensions

The surface dislocation model developed for a

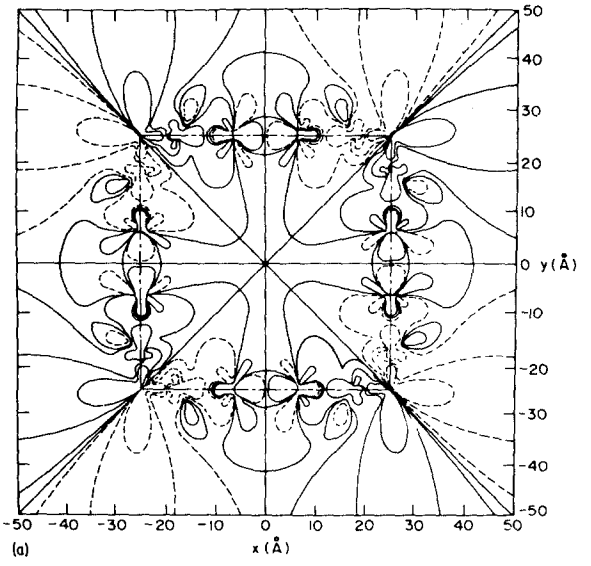

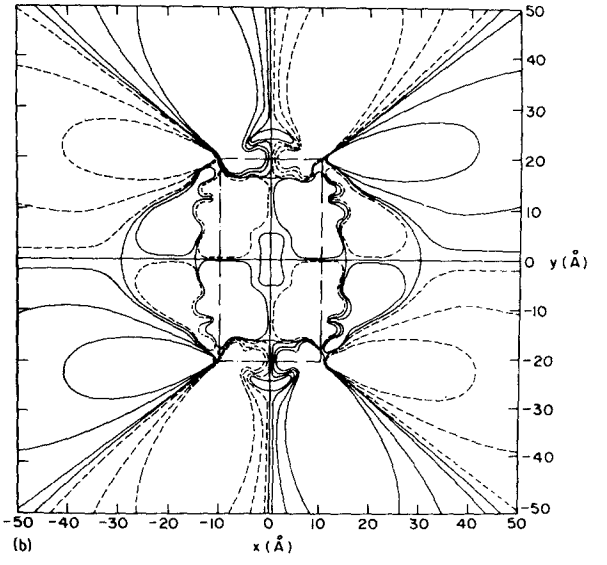

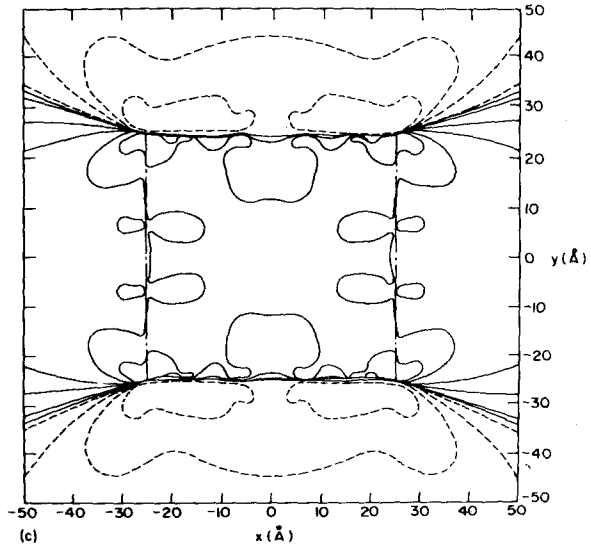

Figure 6 (a) The σ_{xy} component of the stress field due to the array shown in Fig. 5a plotted at various stress levels. Three stress levels plotted in units of $10^{-8} G/4\pi(1-\nu)$ are 0.1, 0.5 and 1. The dotted representation indicates the negative stress levels and the full line representation corresponds to the positive values. A full line between a dotted line and a full line indicates zero stress level. The figure is drawn to scale. (b) Same as (a) except that the array corresponds to Fig. 5b with width equal to 200 Å. (c) The σ_{xx} component of the stress field due to the array shown in Fig. 5a plotted at various stress levels. The four stress levels plotted in units of $10^{-8} G/4\pi(1-\nu)$ are 0.1, 0.5, 1 and 2. The representation of the stress levels is the same as in (6a).

finite solid can easily be extended to a liquid of finite dimensions. In the past, the properties of dislocations have been used to determine viscosity in terms of a heavily dislocated crystal [9]. In order to illustrate the discrete dislocation analysis with respect to the surface tension of a liquid of finite dimensions, a two dimensional circular film is considered, as shown in Fig. 7a. The surface dislocations are distributed uniformly along the circumference of the body.

The circular region is divided into 36 sectors, each containing a dislocation with Burgers vector tangential to the surface. Let the initial radius be r_0 and the sum of the Burgers vectors of all the surface dislocations be $\boldsymbol{b}$. The array shown in Fig. 7a does not have a resultant shear stress component inside the circular region. The hydrostatic pressure due to the array, represented by a constant P, contributes to the strain energy as follows,

$$E_e = P\boldsymbol{b}(r_0 - \boldsymbol{b}/2\pi)/2. \tag{13}$$

The surface energy lost due to the formation of the dislocation array is

$$E_\gamma = \gamma \boldsymbol{b}. \tag{14}$$

The balance of strain energy with loss of surface energy gives

$$\boldsymbol{b} = 2\pi(r_0 - 2\gamma/P), \tag{15}$$

in turn connecting the total Burgers vector of the surface array to the initial radius and the surface energy. The pressure P is a function of the distribution of the surface array. The results of the discrete dislocation analysis are presented for two different liquids, as shown in Fig. 7.

It is now a simple procedure to determine the shape of a drop of liquid lying on the surface of a solid. Fig. 8a is a schematic illustration of the surface dislocation arrays present on the surfaces of the liquid droplet and the finite solid. The array on the surface of the liquid droplet maintains the hydrostatic pressure within the liquid droplet and the two arrays on the surface of the solid maintain the surface stresses on the surface of the solid. The dislocation array at the interface screens the stress components so that only hydrostatic stresses are present in the liquid medium. The angle θ shown in the figure corresponds to the contact angle.

Fig. 8b shows the shape of the droplet determined from a discrete dislocations analysis. The surface arrays on the surfaces of the solid are neglected in order to simplify the calculation. It should also be pointed out that when the dimensions of the finite solid are large compared to that of the liquid region, the Burgers vector of the surface arrays on the solid become very small due to the high shear modulus of the solid.

The computational procedure in the determination of the shape of the droplet consists of an initial circular droplet which is allowed to settle on the surface of a solid and to alter its shape, maintaining constant volume while minimizing the total energy of the configuration. The array shown in Fig. 8b in the liquid medium has no resultant shear stress component. The hydrostatic pressure due to the array represented by a constant P, contributes to the strain energy

$$E_e = \frac{P}{2} \int_{\theta_1}^{\theta_2} [R(\theta) - \boldsymbol{b}(\theta)]\, \boldsymbol{b}(\theta) \mathrm{d}\theta \tag{16}$$

where $R(\theta)$ and θ are the co-ordinates of a point on the surface from the reference co-ordinate system chosen in the liquid medium and $\boldsymbol{b}(\theta)$ is the Burgers vector of the dislocation present on the surface at that point. θ_1 and θ_2 are the angles shown in Fig. 8a. The surface energy lost due to the formation of the surface dislocation array is

$$E_\gamma = \gamma_1 \int_{\theta_1}^{\theta_2} \boldsymbol{b}(\theta) \mathrm{d}\theta \tag{17}$$

where γ_1 is the surface energy of the liquid–vacuum interface. At the interface

$$\gamma_1 \boldsymbol{b}_s \cos\theta_1 = (\gamma_3 - \gamma_2)\boldsymbol{b}_s,$$

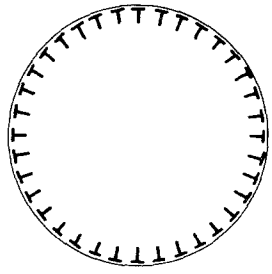

$r_0 = 1000$ Å

$\gamma = 72.5$ $\mu = 1.5 \times 10^9$ $b_i = 0.023$ Å

$\gamma = 480$ $\mu = 2.5 \times 10^9$ $b_i = 0.098$ Å

Figure 7 A two-dimensional circular film of liquid of radius r_0. Surface dislocations each of Burgers vector $\boldsymbol{b}_i$ are spread along the circumference at equal intervals of 10°. The value of $\boldsymbol{b}_i$ for two sets of liquids is shown in the figure.

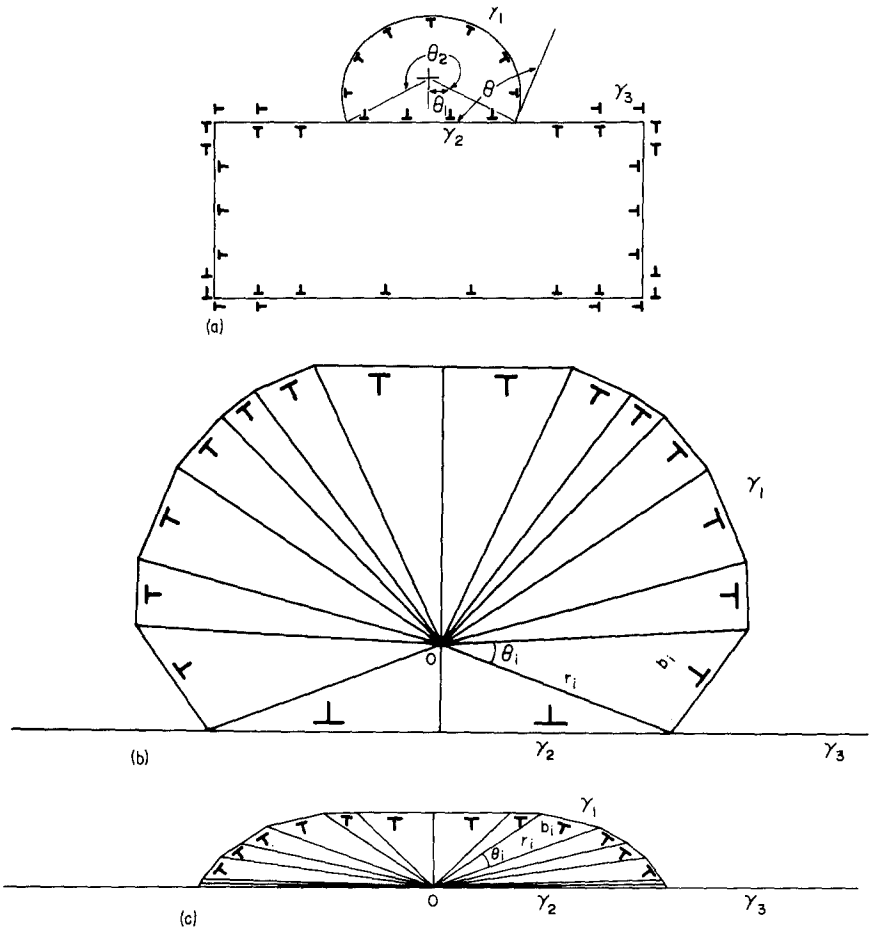

Figure 8 (a) Schematic illustration of the surface dislocation model of a liquid droplet on the surface of a solid of finite dimensions. The surface dislocations on the surface of the liquid have their Burgers vectors tangential to the surface. The two sets of surface dislocation arrays with Burgers vectors mutually orthogonal to each other on the surface of the solid maintain the surface stresses within the solid. The interface array has the Burgers vector parallel to the interface so that the shear stresses from the solid are screened and only hydrostatic stresses are present within the liquid. (b) Shape of a liquid droplet lying on the surface of a solid with contact angle equal to 53°. One half of the region of the droplet is divided into eight sectors. The co-ordinates r_i, θ_i and the Burgers vector $\boldsymbol{b}_i$ of a dislocation in each sector are shown in Table I for the indicated values of γ_1, γ_2 and γ_3. (c) Shape of a droplet of liquid on the surface of a solid with contact angle equal to 124°. The co-ordinates r_i, θ_i and the Burgers vector $\boldsymbol{b}_i$ of a dislocation in each sector are shown in Table II for the indicated values of γ_1, γ_2 and γ_3.

which determines the contact angle θ equal to $180 - \theta_1$. In Equation 18, γ_2 is the surface energy of the liquid–solid interface, γ_3 that of the solid–vacuum interface, and $\boldsymbol{b}_s$ the sum of the Burgers vectors of the dislocations at the solid–liquid interface. When the contact angle θ is 180 degrees, the droplet becomes a two dimensional circular film with $R(\theta) = r_0$, $\boldsymbol{b}(\theta) = \boldsymbol{b}/2\pi$, $\theta_1 = 0$ and $\theta_2 = 2\pi$ so that Equations 13 and 14 are obtained from the above analysis.

In order to facilitate the computation, the area comprising one half of the droplet was divided into eight sectors. Within each sector the Burgers vector of the surface dislocation is tangential to the surface of the droplet. The radius vector r_i and the angle θ_i in each sector are varied along with Burgers vector $\boldsymbol{b}_i$ so that the total energy of the medium remains at its minimum. Table I shows the results of the discrete dislocation analysis and Fig. 8b illustrates the shape of the droplet drawn to scale. The shape of the droplet depends on the relative values of γ_1, γ_2 and γ_3 as indicated in Table I. In particular the shape for $\gamma_3 > \gamma_2$ is shown in Fig. 8c and Table II gives the results obtained by minimization of the total energy. The present results agree closely with the classical

TABLE I The radius vector r_i, the angle θ_i and the Burgers vector b_i in each of the eight sectors in one half of the liquid droplet. $\gamma_1 = 72.5, \gamma_2 = 80$ and $\gamma_3 = 40$

	1	2	3	4	5	6	7	8
r_i(Å)	500	1453	1740	1782	1782	1790	1797	1782
θ_i(radians)	1.219	0.414	0.275	0.317	0.223	0.124	0.136	0.436
b_i(Å)	0.001	0.747	0.240	0.001	0.002	0.003	0.130	0.067

methods of analysis [10] if it is noted that the Burgers vector of the surface dislocations is very small compared to the radius of curvature in Equation 15 so that $r_0 = 2\gamma/P$.

The results of the discrete dislocation analysis when applied to solids and liquids illustrates the use of surface dislocations in representing the resultant stress field that arises due to surface tension. The surface dislocation representation includes both the strain energy and the surface energy in the total energy of the medium.

4.2. Numerical analysis of the dislocation configuration associated with a two-phase interface

The structure of a semi-coherent interface in terms of the rearrangement of interface dislocations and partial annihilation with the misfit dislocation, as elucidated earlier, will be analysed using the discrete dislocation method of analysis. The method of continuous distribution of dislocations has already been employed earlier to determine the structure of a semi-coherent interface [2]. However, the frictional stress required to prevent the complete annihilation of interface dislocations with the misfit dislocations has been assumed to be of a simple form so as to obtain closed form solutions for the relevant singular integral equation. It is to be realized that the frictional stress and interface energy are not different entities and should be related by

$$\tau_f b_i = \gamma \qquad (19)$$

where τ_f is the frictional stress, b_i the Burgers vector of the dislocation responsible for the formation of the step and γ the interfacial energy. The frictional stress required to move a dislocation can be assumed to be of the familiar form [2],

$$\tau_f = (\alpha G_1 b_m/2\pi d) \sin (2\pi\Phi/b_m) \qquad (20)$$

where Φ is the disregistry produced between any two atoms across the interface, b_m the Burgers vector of the misfit dislocation, d the repeat distance between misfit dislocations and α, a parameter used to change the magnitude of the frictional stress. Analytical solutions to the integral equation giving the equilibrium distribution of interface dislocations could not be obtained using Equation 20. Therefore, the discrete dislocation method was employed to determine these equilibrium configurations. The dislocation model employed is shown in Fig. 3g where three misfit dislocations along with the interface dislocations around them are considered. The total energy, E_T, of the configuration in the centre consisting of a misfit dislocation and the accompanying interface dislocations is minimized. In particular

$$E_T = E_S + E_{I,M} + E_{I,I} + E_F, \qquad (21)$$

where E_S is the self energy of the interface array and the misfit dislocation, $E_{I,M}$ the interaction energy of the interface array with the misfit dislocations, $E_{I,I}$ the interaction energy of each dislocation in the interface array with other dislocations and E_F the frictional energy expended in moving the interface array against τ_f. In the determination of the interaction energy terms with neighbouring arrays, care should be exercised in considering only one half of the energy terms since the interaction energy is shared by both the regions. The frictional stress acting on each dislocation depends on the step already produced by the movement of preceding interface dislocations. The resultant dislocation configuration obtained using $G_1 = 7.14 \times 10^{11}$ dyn cm^{-2} and

TABLE II The radius vector r_i, the angle θ_i and the Burgers vector b_i in each of the eight sectors in one half of the liquid droplet. $\gamma_1 = 72.5, \gamma_2 = 60, \gamma_3 = 80$

	1	2	3	4	5	6	7	8
r_i(Å)	14	3382	3154	2923	2595	2005	1591	1162
θ_i(radians)	1.568	0.067	0.141	0.087	0.122	0.248	0.165	0.744
b_i(Å)	0	0.0017	0.2074	0.1643	0.0010	0.0010	0.1555	0.1497

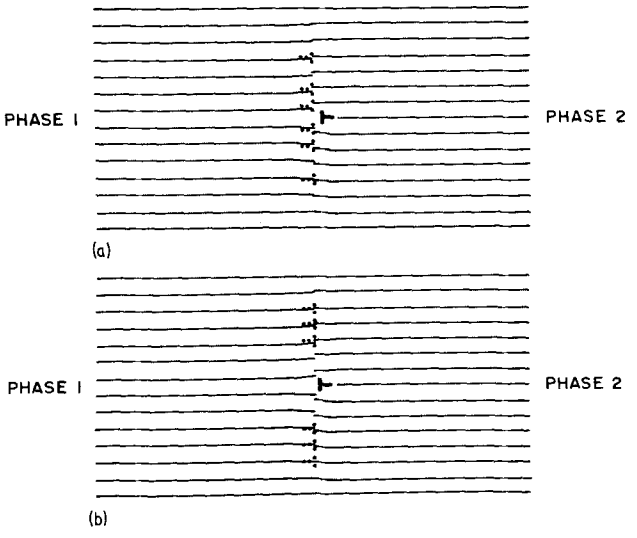

Figure 9 (a) The structure of the interface consisting of the interface and misfit dislocations in the semi-coherent state for $G_2 = G_1$ and $\alpha = 1$. (b) As (a) but with $\alpha = 2$.

$\nu_2 = \nu_1 = 0.333$ is shown in Figs. 9 to 12 for two combinations of the shear moduli of the two phases and various values of α. The step height produced by the movement of each interface dislocation is also shown. The interface dislocations are found to stop at positions where a step would have been created if further movement of the dislocation took place and thus expend frictional energy or create equivalent interfacial energy. The number of interface dislocations remaining after annihilation increases with increasing friction as illustrated by the increase in value of α and decreases with increasing shear modulus of the second phase G_2.

While the general results of the present calculations employing discrete dislocation methods agree with those obtained earlier [2], the details of the dislocation configuration at the interface are different due to different form of frictional stress used in the present analysis. It should also be pointed out that the misfit dislocation is assumed to be nucleated at the interface in the present calculations.

5. Conclusions

The formation of any new surface involves the breaking of atomic bonds, which in turn increases the energy of the body. In order to minimize this surface energy, the total area of the surface decreases, in turn giving rise to an internal stress within the body. It is shown that the decrease in surface area is equivalent to the introduction of a continuous distribution of surface dislocations on the surface of the body. It is the surface dislo-

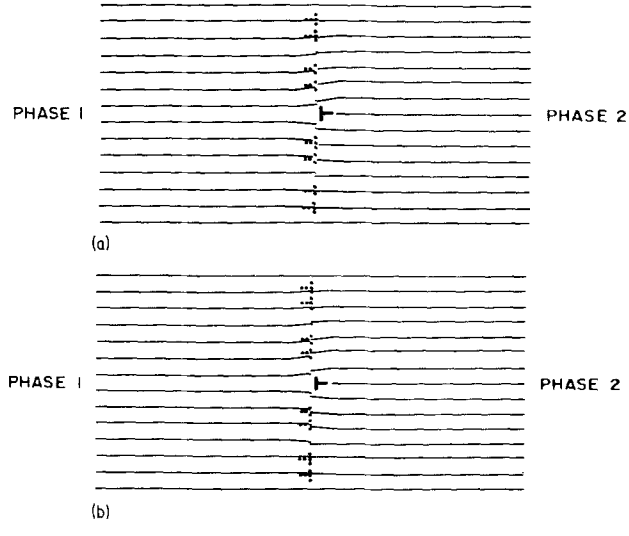

Figure 10 (a) As Fig. 9a but with $\alpha = 5$. (b) As (a) but with $\alpha = 10$.

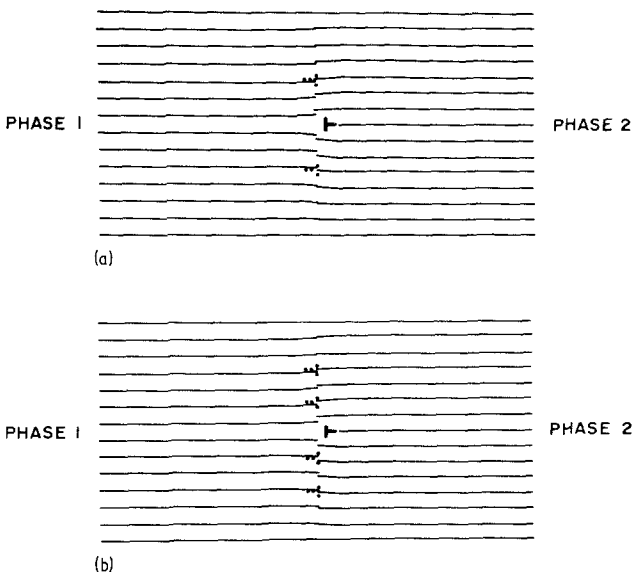

Figure 11 (a) As Fig. 9a except $G_2 = 10G_1$ and $\alpha = 1$. (b) As (a) but with $\alpha = 2$.

cations which give rise to the strain energy within the body. Equilibrium is established when the increase in this strain energy is just balanced by the corresponding decrease in surface energy occasioned by these surface dislocations. This decrease in surface energy is also related to the stresses acting on the free surface of the body, i.e. surface tension. In general, for a solid with an arbitrary shaped surface, all components of stress are present within the body, whereas for a liquid, no shear stress components are allowed, so that the surface of the liquid must adjust its shape accordingly. Numerical calculations have been carried out for all of the cases as well as for liquid droplets in contact with solids. These same free surface energy considerations apply also to external surfaces such as interphase boundaries. Under these conditions, interphase boundary dislocations, which are the equivalent of surface dislocations, are formed. Rearrangement of these boundary dislocations can occur so as to lower the elastic strain energy, but only at the expense of increasing the surface energy of such boundaries. The resistance to the motion of these dislocations is equivalent to a lattice friction stress acting within the boundary. This detailed model of an

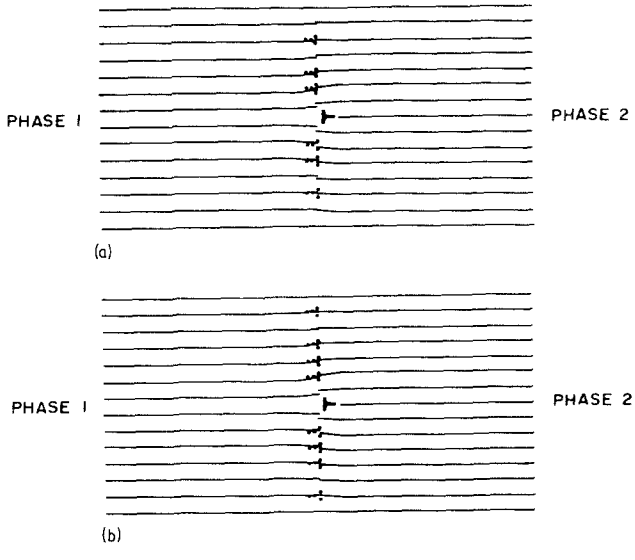

Figure 12 (a) As Fig. 11a but with $\alpha = 5$. (b) As (a) but with $\alpha = 10$.

interphase boundary allows an exact description to be given for a fully coherent, a fully incoherent and a partially coherent interface.

Acknowledgements

The computer time for the project was supported in full through the facilities of the Computer Science Center of the University of Maryland. Financial support for the present study was provided by the U.S. Department of Energy under Contract No. AT-(40-1)-3935.

References

1. K. JAGANNADHAM and M. J. MARCINKOWSKI, *Phys. Stat. Sol.* **50** (1978) 293.
2. *Idem, J. Appl. Phys.* **48** (1977) 3788.
3. *Idem, Mat. Sci. Eng.* (to be published).
4. M. J. MARCINKOWSKI, "Fundamental Aspects of Dislocation Theory", NBS Special Publication No. 317, Vol. 1, edited by J. A. Simmons, R. deWit and R. Bullough (1970) 531.
5. Y. C. FUNG, "Foundations of Solid Mechanics" (Prentice Hall, New Jersey, 1965).
6. M. J. MARCINKOWSKI, "Unified Theory of the Mechanical Behaviour of Matter", (Wiley, New York, 1978).
7. *Idem, Acta Mech.* (to be published).
8. C. HERRING, "Physics of Powder Metallurgy", edited by W. Kingston (McGraw Hill, New York, 1951) Ch. 8, p. 143.
9. W. SHOCKLEY, "L'Etat Solide", p. 431.
10. A. H. COTTRELL, "The Mechanical properties of Matter" (Wiley, New York, 1964) Ch. 8.

Received 20 October and accepted 20 November 1978.